10098 *Biochemistry* **2009,** *48,* 10098–10105
DOI: 10.1021/bi901104d

BIOCHEMISTRY
including biophysical chemistry & molecular biology
Article

Structural Basis of the Hydride Transfer Mechanism in F_{420}-Dependent Methylenetetrahydromethanopterin Dehydrogenase†

Katharina Ceh,‡ Ulrike Demmer,‡ Eberhard Warkentin,‡ Johanna Moll,§ Rudolf K. Thauer,§ Seigo Shima,§ and Ulrich Ermler*,‡

‡*Max-Planck-Institut für Biophysik, Max-von-Laue-Strasse 3, D-60438 Frankfurt am Main, Germany, and* §*Max-Planck-Institut für terrestrische Mikrobiologie, Karl-von-Frisch-Strasse, D-35043 Marburg, Germany*

Received June 30, 2009; Revised Manuscript Received September 16, 2009

ABSTRACT: F_{420}-dependent methylenetetrahydromethanopterin (methylene-H_4MPT) dehydrogenase (Mtd) of *Methanopyrus kandleri* is an enzyme of the methanogenic energy metabolism that catalyzes the reversible hydride transfer between methenyl-H_4MPT^+ and methylene-H_4MPT using coenzyme F_{420} as hydride carrier. We determined the structures of the Mtd−methylene-H_4MPT, Mtd−methenyl-H_4MPT^+, and the Mtd−methenyl-H_4MPT^+-$F_{420}H_2$ complexes at 2.1, 2.0, and 1.8 Å resolution, respectively. The pterin−imidazolidine−phenyl ring system is present in a new extended but not planar conformation which is virtually identical in methenyl-H_4MPT^+ and methylene-H_4MPT at the current resolution. Both substrates methenyl-H_4MPT^+ and $F_{420}H_2$ bind in a face to face arrangement to an active site cleft, thereby ensuring a direct hydride transfer between their C14a and C5 atoms, respectively. The polypeptide scaffold does not reveal any significant conformational change upon binding of the bulky substrates but in turn changes the conformations of the substrate rings either to avoid clashes between certain ring atoms or to adjust the rings involved in hydride transfer for providing an optimal catalytic efficiency.

Methylenetetrahydromethanopterin (methylene-H_4MPT)[1] dehydrogenase is an enzyme in the C_1 metabolism of methanogenic archaea, methane-oxidizing archaea, sulfate-reducing archaea, and some methylotrophic bacteria that catalyzes the reversible hydride transfer between methenyl-H_4MPT^+ and methylene-H_4MPT.

The one-carbon carrier H_4MPT is built up of a reduced pterin connected to an arylamine via a methylene group (Figure 1). It covalently binds one-carbon units in the oxidation states of formate, formaldehyde, and methanol via the N^5 atom of the pterin and the N^{10} atom of the arylamine (*1*−*3*). The hydride donors for the methylene-H_4MPT dehydrogenase reactions are in the methanogens coenzyme $F_{420}H_2$ and H_2, in methane-oxidizing and sulfate-reducing archaea $F_{420}H_2$, and in methylotrophic bacteria NAD(P)H. F_{420} is a flavin analogue (Figure 1) where primarily the N^5 atom of the isoalloxazine ring is replaced by a carbon atom that results in a redox behavior more similar to that of NAD(P)H (*4*). In contrast to hydride transfer reactions with FAD and NADP, those with F_{420} exclusively take place at its *si*-face for unknown reasons (*1*). The structures of F_{420}, H_2, and NAD(P)H-dependent methylene-H_4MPT dehydrogenase (*5*−*7*) completely differ, but all of them catalyze a hydride transfer reaction via a ternary complex mechanism (implying that the hydride donor and acceptor are in van der Waals contact with each other) and are *re*-face specific catalysts with respect to C14a of methylene-H_4MPT (*8*) (Figure 1).

A related hydride transfer reaction is catalyzed by methylenetetrahydrofolate dehydrogenase using tetrahydrofolate as C_1 carrier and NAD(P)H as electron donor (*9*). H_4MPT is mainly distinguished from the structurally related tetrahydrofolate by an electron-donating methylene group compared to an electron-withdrawing carbonyl group linked to the arylamine ring. This difference is also the main reason why the redox potential of methenyl/methylene-H_4MPT (∼−390 mV) and methylene/methyl-H_4MPT (∼−320 mV) couples are about 100 mV more negative than that of the corresponding tetrahydrofolate complexes (*10*). Interestingly, H_4MPT- and tetrahydrofolate-dependent enzymes (catalyzing analogous reactions) and the enzyme machinery biosynthesizing H_4MPT and tetrahydrofolate are structurally unrelated, suggesting an independent development of the one-carbon carriers as two solutions of a convergent evolutionary process.

The presented investigations are based on Mtd from *Methanopyrus kandleri*, which is a hyperthermophilic methanoarchaeon (growth temperature 98 °C) with high cellular concentration of cyclic 2,3-diphosphoglycerate (1.1 M) (*11*). Methanogens perform the terminal process of the anaerobic decomposition of organic material by metabolizing several one-carbon compounds (i.e., CO_2 and methanol) and acetate in fresh water environments. The biochemistry of their energy metabolism is based on a stepwise reduction of cofactor-bound and activated one-carbon compounds to methane (*1*). Biochemical studies on Mtd from several methanogenic organisms revealed that the protein consists of one type of subunit with a molecular mass of 30−35 kDa and lacks a prosthetic group (*12*−*14*). An X-ray structure of Mtd from *M. kandleri* at 1.54 Å resolution revealed a homohexameric complex organized as a dimer of trimers (Figure 2). Each subunit is built up of a large α,β domain and a helical bundle domain with

†This work was supported by DFG Project ER222/-2 and the Max Planck Society.

*To whom correspondence should be addressed. Phone: ++49-(0)69-6303-1054. Fax: ++49-(069)-6303-1002. E-mail: ulrich.ermler@mpibp-frankfurt.mpg.de.

[1]Abbreviations: H_4MPT, tetrahydromethanopterin; Mtd, methylene-H_4MPT dehydrogenase.

 Published on Web 09/18/2009

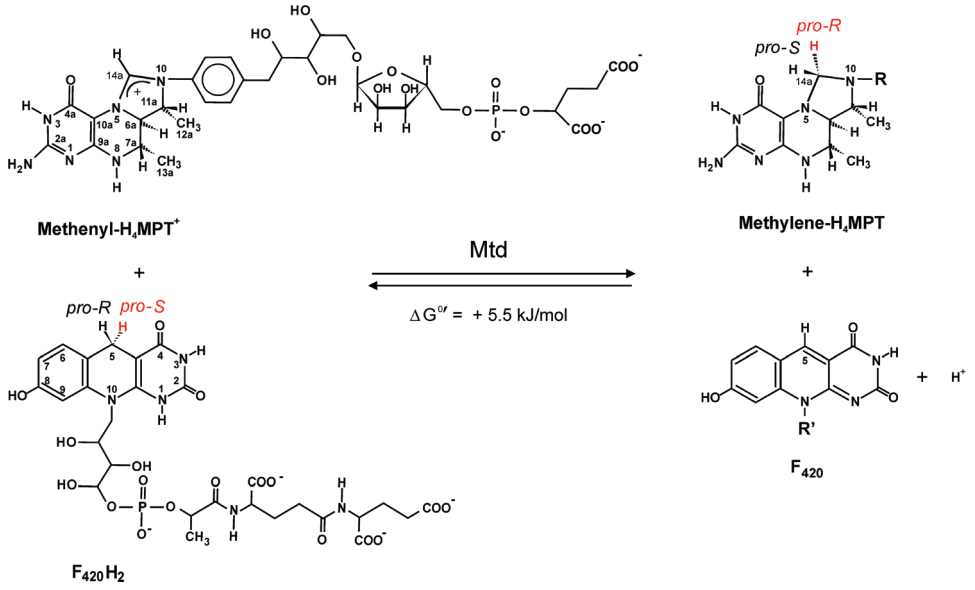

FIGURE 1: Catalytic reaction of Mtd. The hydride in the *proS* position of $F_{420}H_2$ is reversibly transferred to the *proR* position of methenyl-H_4MPT^+. The one-carbon carrier H_4MPT is structurally highly related to tetrahydrofolate. The hydride donor/acceptor F_{420} is a deazaflavin where the N5 atom is replaced by a carbon leading to redox properties that are similar to those of NAD(P).

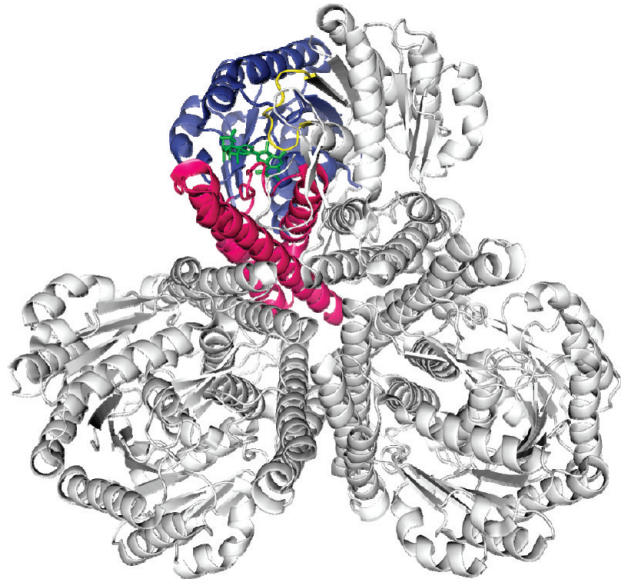

FIGURE 2: Structure of the homohexameric enzyme complex Mtd of *M. kandleri* (gray) in complex with methenyl/ylene-H_4MPT. Each subunit is composed of an α,β domain (blue) and an α-helical bundle domain (magenta) with a short C-terminal extension. Mtd has no structural similarity to any other H_4MPT and tetrahydofolate-dependent enzyme. The active site is located in a crevice between the two domains of one subunit and is covered by a loop segment (yellow) of the counter subunit. Methenyl/ylene-H_4MPT (green) sits in the crevice.

a short C-terminal β-sheet segment (*5*). No structural similarities are detectable to other H_4MPT- and F_{420}-dependent enzymes. Kinetic studies on Mtd of *M. kandleri* resulted in a specific activity of 3700 units/mg and K_m values of 30 μM for F_{420} and of 40 μM for methylene-H_4MPT measured at 1 M $(NH_4)_2SO_4$ and at temperatures of 65 °C (*15*).

The structural basis of the hydride transfer reaction mechanism between complex ring-shaped cofactors is established for FAD and NAD(P)(*16*), FAD and methylene-H_4F (*17*), F_{420} and NADP (*18*), and H_4F and NADP (*19*). The presented study reveals the first example where both a H_4MPT derivative and F_{420} are bound to an enzyme structure. We describe the conformations of methylene-H_4MPT, methenyl-H_4MPT^+, and $F_{420}H_2$ as well as their interactions to the polypeptide of Mtd from *M. kandleri* and discuss the pronounced rigidity of the substrate-binding crevice and the hydride transfer process.

MATERIALS AND METHODS

Production and Crystallization. Mtd from *M. kandleri* was overproduced in *Escherichia coli* and purified by a Q-Sepharose, Source 15 Phenyl, and a Superdex 200 column which slightly deviates from the protocol described earlier (*15*, *20*). The protein was concentrated to ca. 35 mg/mL in 10 mM MES, pH 5.5, and was stored at −80 °C until further use. H_4MPT and F_{420} were purified from *Methanothermobacter marburgensis* (DSM 2133)(*21*) and stored at a concentration of about 30 mM in 10 mM MES, pH 5.5.

Crystallization trials were performed with the hanging drop vapor diffusion method using a sparse matrix crystallization kit (Jena Bioscience) for initial screening. The experiments were carried out in an anaerobic tent under an atmosphere of 95% N_2/5% H_2 under low-intensity red light conditions since H_4MPT is sensitive to O_2 and light. The enzyme solution consists of 15 mg/mL protein and 5 mM methenyl/ylene-H_4MPT in 10 mM MOPS, pH 7.0, for the binary complexes and of 15 mg/mL protein and 5 mM methylene-H_4MPT in 10 mM MOPS, pH 7.0, and 5 mM F_{420} for the ternary complex. Crystals were obtained at a temperature of 18 °C after mixing equal volumes of the enzyme solution and the reservoir solution containing ca. 30% (w/v) PEG 400, 0.1 M MES, pH 6.5, and 0.1 M sodium acetate.

Structure Determination. Data for the Mtd−methylene-H_4MPT, Mtd−methenyl-H_4MPT^+, and Mtd−methenyl-H_4MPT^+−$F_{420}H_2$ complexes were collected at the SLS-PX2 beamline in Villigen, Switzerland, to a resolution of 2.1, 2.0, and 1.8 Å, respectively. Processing and scaling were performed using the programs HKL (*22*) and XDS (*23*), respectively. The structures were solved by the molecular replacement method using the programs AMORE (*24*) and PHASER (*25*) and the coordinates of Mtd from *M. kandleri* without cofactors (*5*) as first

Table 1: Data Collection and Refinement Statistics

	data set		
	Mtd + methenyl-H_4MPT^+ + $F_{420}H_2$	Mtd + methylene-H_4MPT	Mtd + methenyl-H_4MPT^+
	(A) Data Collection		
wavelength (Å)	0.9918	1.008	1.008
space group	$P2_1$	$P2_1$	$P2_1$
unit cell parameters			
a, *b*, *c* (Å)	61.1, 165.5, 93.6	62.8, 167.7, 95.9	103.4, 167.2, 122.5
β (deg)	99.1	101.3	113.6
no. of hexamers in the asym unit	1	1	2
resolution range (Å) (highest shell)	92.5−1.8 (1.9−1.8)	94.0−2.1 (2.2−2.1)	112.5−2.0 (2.1−2.0)
redundancy	3.4 (2.6)	3.9 (3.9)	4.0 (3.2)
completeness (%)	95.7 (94.9)	96.7 (96.4)	99.2 (77.6)
R_{sym} (%)	7.4 (41.1)	4.8 (53.0)	6.2 (51.1)
$I/\sigma(I)$	15.6 (2.8)	16.1 (2.9)	14.9 (2.7)
	(B) Refinement		
resolution limit (Å)	92.45−1.80	94.02−2.10	112.51−2.0
R_{work}/R_{free} (%)	19.0/22.8	19.7/22.4	17.0/20.2
no. of residues	1698	1698	3396
no. of solvent molecules	773	301	1248
rmsd bond lengths (Å)	0.014	0.017	0.016
rmsd bond angles (deg)	1.6	1.6	1.7
average *B* (Å^2): protein, methenyl/ylene-H_4MPT, $F_{420}H_2$, solvent	21.9, 30.7, 36.0, 31.8	12.6, 32.1, −, 17.6	22.3, 36.5, −, 31.9

search model. Iterative cycles of refinement and manual model building were performed with programs REFMAC5 (*26*) and COOT (*27*). The initial cycles of refinement were carried out without the cofactors modeled in the structure. Electron density for methenyl/ylene-H_4MPT and F_{420} could be clearly identified, allowing its incorporation using COOT. TLS refinement, treating each monomer as a separate TLS group, maximum likelihood minimization with isotropic *B*-value refinement, and several modifications of the geometry files of the substrate lead to the final result listed in Table 1. Structure interpretation is based on normalized $2F_o - F_c$, $F_o - F_c$, and the corresponding omit electron density maps; the σ value is defined as the rms deviation from their mean density. The quality of the model was checked with the program PROCHECK (*28*). Figures 2−5 are produced by PYMOL (DeLano Scientific).

RESULTS AND DISCUSSION

Structural Basis. Mtd from *M. kandleri* was structurally characterized in complex with methylene-H_4MPT, with methenyl-H_4MPT^+, and with both methenyl-H_4MPT^+ and coenzyme F_{420}. For simplification, we will use the name methenyl/ylene-H_4MPT for describing aspects common in the oxidized and reduced forms of the C_1 carrier. To prevent decomposition of the methenyl/ylene-H_4MPT, crystallization has to be performed under anaerobic and red light conditions. Phases were determined by the molecular replacement method using the structure of the substrate-free enzyme (in a selenomethionine form) as model (*5*). The binary Mtd−methenyl/(ylene)-H_4MPT complex was refined to an *R* and R_{free} factor of 16.5% (19.9%) and 21.1% (22.7%) in the resolution range 112.5−2.0 (94.0−2.1) Å and the ternary Mtd−methenyl-H_4MPT^+−$F_{420}H_2$ complex to an *R* and R_{free} factor of 19.0% and 22.8% in the resolution range 92.5−1.8 Å, respectively (Table 1). The overall structure of the substrate-free and substrate-bound enzymes are nearly identical, documented by rms values of ca. 0.3 Å calculated for 100% of the C_α atoms of the homohexamer (*29*). Obviously, no significant substrate-induced large-scale rearrangements of subunits, domains, or larger segments occur. Methenyl/ylene-H_4MPT is highly occupied (80−100%) in the binary methenyl-H_4MPT^+ and in the ternary complex but significantly lower (40−50%) in the methylene-H_4MPT complex (Figure 3A−C). The occupancy of F_{420} in the ternary complex varies between 60% and 80% in the six monomers of the asymmetric unit. The following analysis is therefore related to the active site with the highest occupied F_{420} (Figure 3D). The structure of the ternary complex does not allow a definitive distinction between methenyl-H_4MPT^+ and methylene-H_4MPT and between F_{420} and $F_{420}H_2$, respectively, as their structures are similar (see below). Even a mixture of all compounds cannot be excluded. From a thermodynamic point of view the presence of methenyl-H^4MPT^+ and $F_{420}H_2$ in the ternary complex is more likely as the equilibrium of the reaction is on their side at pH 6.5 where the analyzed crystals have been grown. However, the catalytic activity is low or even zero at the crystallization conditions due to the absence of lyotropic salts and the low temperature.

Substrate Binding Site. Methenyl/ylene-H_4MPT and F_{420} are embedded into a crevice between the α,β and the helical bundle domains shielded from the top by a loop segment following α-helix 14:25 of the counter subunit (Figure 2 and 4). The pterin, imidazolidine, and phenyl ring system of methenyl/ylene-H_4MPT is flanked on its *si*-face by the segment (122−133) linking the two domains and by α-helix 133:152 and on its *re*-face by the C-terminal end of β-strands 4:10 and 33:39 of the central β-sheet and by F_{420}. The deazaisoalloxazine ring of F_{420} is sandwiched between the C-terminal end of the central β-sheet at its *re*-face and essentially methenyl/ylene-H_4MPT at its *si*-face. The binding site of F_{420} is shortened by the loop following β-strand 33:39 such that F_{420} is less

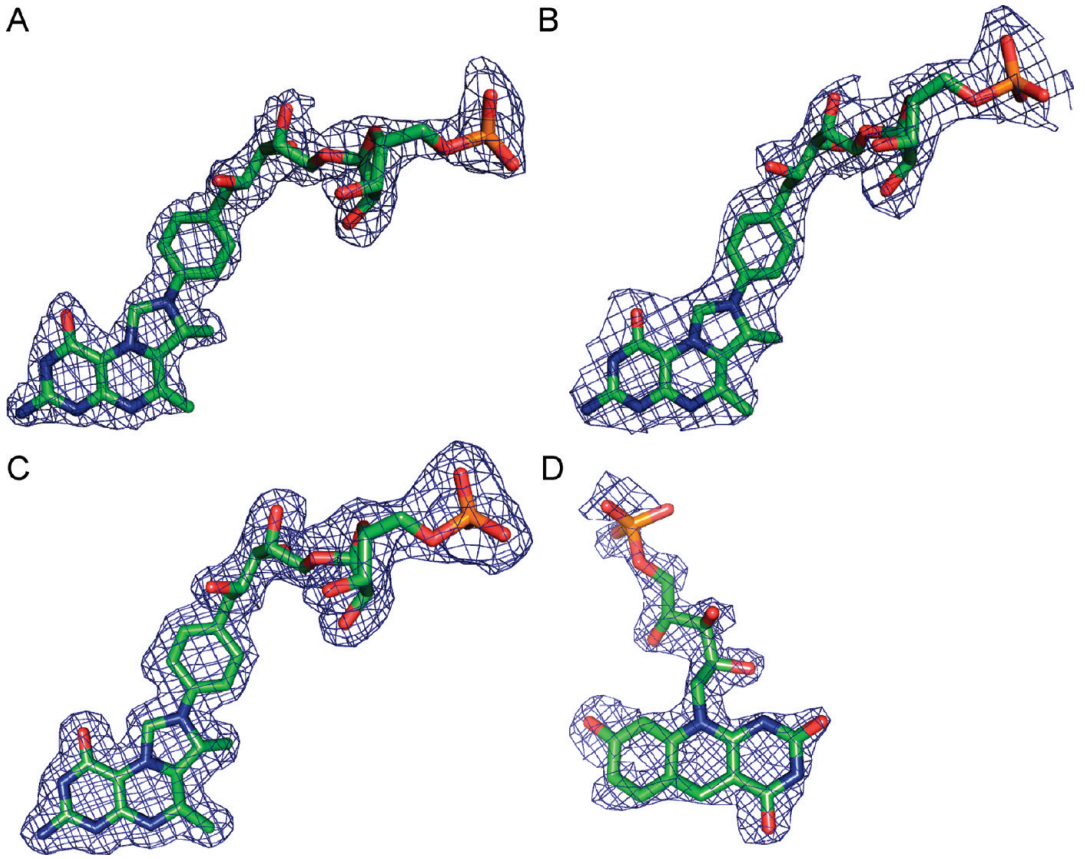

FIGURE 3: $2F_o - F_c$ omit electron density of the substrates. (A) Methenyl-H_4MPT^+ of the binary complex at 2.0 Å resolution; $\sigma = 1.0$. (B) Methylene-H_4MPT of the binary complex at 2.1 Å resolution; $\sigma = 0.8$. (C) Methenyl-H_4MPT^+, $\sigma = 1.0$. (D) F_{420}, $\sigma = 0.8$ at 1.8 Å resolution in the ternary complex. The ring system of methenyl/ylene-H_4MPT is present in an extended conformation, the pyrimidinone and phenyl rings being parallel to each other. Methenyl/ylene-H_4MPT is curved at the ribitol group. F_{420} is present in a butterfly conformation.

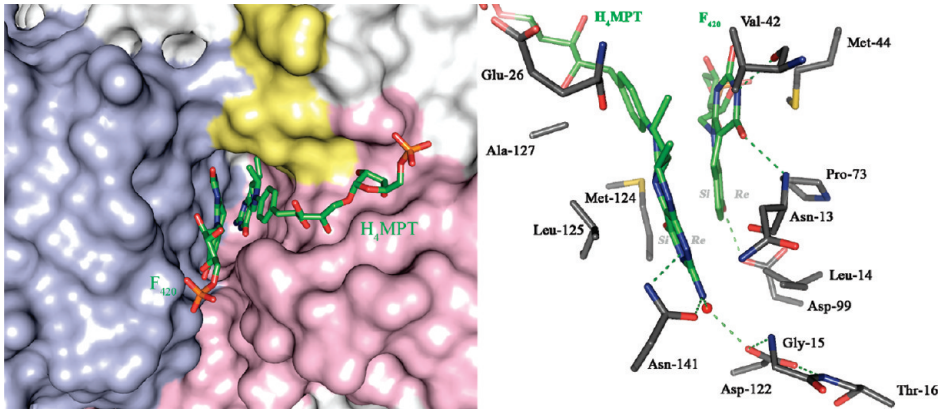

FIGURE 4: Binding site of the substrates methenyl-H_4MPT^+ and $F_{420}H_2$. (A, left) Molecular surface representation of the active site crevice formed by segments of the α,β domain (light blue), the α-helical bundle domain (light magenta), and a loop segment of the counter subunit (yellow). Methylene-H_4MPT and F_{420} shown as stick models (C, green; O, red; N, blue; P, orange) face each other, and the pyridine ring of F_{420} and the imidazolidine ring of methenyl-H_4MPT^+ partly sit upon each other. (B, right) Protein−substrate interactions based on the structure of the ternary complex. Pro73 and Leu125 might compress the hydride-transferring atoms C5 and C14a against each other and induce thereby an orbital overlap that enhances catalysis.

deeply buried into the crevice than methenyl/ylene-H_4MPT (Figure 4). The tails of both substrates are directed toward the crevice entrance but do not contact each other.

Surprisingly, the binding of the two bulky substrates is not accompanied by any significant conformational change of main and side chain atoms of the protein, which indicates an extreme example of a preformed binding site. An explanation of this finding is offered by the multiple connections between the protein interior and the exposed residues forming the geometry of the crevice. Thus, the pterin−imidazolidine−phenyl ring system of methenyl/ylene-H_4MPT is attached to a wall composed of the side chains of Leu125, Met137, Tyr140, and Leu144. All of them are directly linked to the hydrophobic core of the helical domain further stabilized by oligomeric interactions within the multisubunit 12-helix bundle (Figure 2). The other wall is formed by short loops following β-strands 4:10, 33:39, 67:71, and 94:99 of the rigid central β-sheet that is further fixed by association with the corresponding β-sheet of the partner monomer (Figure 2).

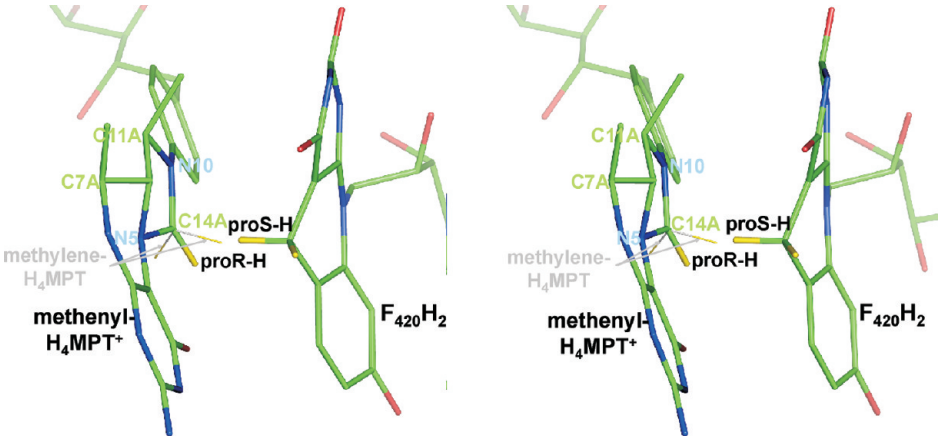

FIGURE 5: Stereospecific hydride transfer of the *proS* hydride bound to C5 of $F_{420}H_2$ to the *proR* side of the C14a atom of methenyl-H_4MPT$^+$. The hydrogen atoms (in yellow) were calculated based on structural data of methenyl-H_4MPT$^+$ and $F_{420}H_2$ of the ternary complex. Assuming the same structure for methylene-H_4MPT the hydrogens of the C14a atom are also calculated and shown as thin lines. The distance between the *proS* hydride of $F_{420}H_2$ and the potential *proR* hydride of methylene-H_4MPT is ca. 0.5 Å.

The structure of the loop segment of the counter subunit that is in van der Waals contact to several atoms of the imidazolidine and tetrahydropyrazine rings via Asp25, Glu26, and Arg27 is maintained by an extended ionic network built up of the side chains of Lys43 and Arg129 of the considered subunit and of Asp25, Glu26, Arg27, Asp29, Arg30, Asp162, and His266 of the counter subunit.

Binding of Methenyl/ylene-H4MPT. Methenyl-H_4MPT$^+$ or methylene-H_4MPT can be clearly identified in the active site crevices as well-shaped electron density is visible between the pterin ring and the phosphate group in all three structures (Figure 3A−C). Solely, the hydroxyglutarate group is highly disordered. The temperature factor slowly increases from the pterin ring (20 Å^2) at the bottom of the crevice toward the ribitol group (28 Å^2) and raises rapidly from the ribose (32 Å^2) to the phosphate group (46 Å^2). The *B*-values were taken from a highly occupied methenyl-H_4MPT$^+$ of the ternary complex. In all three complex structures the pterin, imidazolidine, and phenyl ring systems are highly extended and fill out the complete lengths of the crevice which has dimensions of ca. 15 × 10 × 7 Å^3 (Figure 4A). After the phenyl group the methenyl/ylene-H_4MPT molecule curves and thereby remains associated with the polypeptide chain at one side. The expanded arrangement of the pterin, imidazolidine, and phenyl ring systems of methenyl/ylene-H_4MPT is surprising since methylene-H_4MPT in solution (*8*) and especially in complex with the formaldehyde-activating enzyme (*30*) revealed a sharp kink between the pterin and the imidazolidine rings. A similar kink was found in methylene-H_4F of thymidylate synthase (*31*) and in methyl-H_4F of methylene-H_4F reductase (*17*). We assume that the outstretched conformation independent of the presence of methenyl-H_4MPT$^+$ and methylene-H_4MPT is a consequence of the restraints imposed by the rigid polypeptide scaffold forming the crevice.

A detailed analysis of the conformation of the rings, in particular, of the imidazolidine ring, is based on omit maps and on test calculations with imidazolidine rings in different conformations. Considering that atomic differences below ca. 0.2 Å are not reliably detectable at the current resolutions, no significant differences between methenyl-H_4MPT$^+$ and methylene-H_4MPT are visible. In all three structures the tetrahydropyrazine and imidazolidine rings are not planar in contrast to the pyrimidinone and phenyl rings (Figures 3A−C and 5). The C6a atom of the tetrahydropyrazine ring sits at the *re*-face and the C7a atom at the *si*-face of the pyrimidinone plane. The C13a methyl group attached to the C7a atom points to the *re*-face, which clearly confirms the puckered ring conformation. The nonplanarity of the imidazolidine ring is characterized by the C11a atom slightly shifted toward the *si*-face of the ring system and its methyl group (not present in H_4F), which is oriented ca. 65° out of the ring plane toward F_{420} on the *re*-face (Figures 3A−C and 5). While the N5, C10a, C6a, and C14a atoms are found in a tetrahedral arrangement, the N10, C11a, C14a, and C1b (of phenyl) atoms appear to be arranged more but not completely planar. In the nonplanar conformation the lone pair of N10 is synclinal to the *proR* C14a-H bond, which was also found for methylene-H_4MPT in solution by NMR studies (*8*).

The interactions between the polypeptide chain and methenyl-H_4MPT$^+$ are characterized by a large number of van der Waals contacts to equally distributed residues shaping a binding site that accurately accommodates the pterin, imidazolidine, and phenyl rings. Notably, the methyl groups linked to the tetrahydropyrazine and imidazolidine rings are in van der Waals contact to residues 26−28 of the counter subunit (Figures 2 and 4B). Binding strength and rigidity is additionally provided by several specific hydrogen bonds. For example, invariant Asn141 is hydrogen bonded to the N1 atom and the NH_2 group of the pyrimidinone ring in a bidentate manner via its amide side chain (Figure 4B). Another conserved residue involved in pterin binding is Asp122 that binds to the N3 and NH_2 atoms of the pyrimidinone ring via a firmly bound solvent molecule. Asp122 also links the two stretches 11:14 and 122:133 that sandwich the pterin ring of methenyl/ylene-H_4MPT by two hydrogen bonds to the amino groups of Thr16 and Gly15 positioned at the positively charged N-terminal end of helix 14:25 (Figure 4B). Both Asp122 and Asn141 are part of the most conserved segment of the whole protein located at the *si*-face of methenyl/ylene-H_4MPT. Glutamate (aspartate) and glutamine (or asparagine) are frequently used residues in pterin-dependent enzymes to bind polar pyrimidinone atoms (*30*, *32*).

Binding of Coenzyme $F_{420}H_2$. Coenzyme $F_{420}H_2$ is visible in the electron density map of the ternary complex from the deazaisoalloxazine ring to the first glutamate group (Figure 3D). The deazaisoalloxazine ring is embedded most deeply into the crevice and has the lowest temperature factor (27 Å^2; occupancy = 80%); the ribitol and the phosphate groups are

directed linearly toward the entrance. The phosphate group is already highly solvent exposed; the residual fraction of $F_{420}H_2$ has no contact to the protein (Figure 4A) and is essentially disordered. The deazaisoalloxazine ring of $F_{420}H_2$ and the phenyl−imidazolidine−tetrahydropyrazine rings of methenyl-H_4MPT^+ are arranged roughly perpendicular to each other, the central pyridine ring being partly stacked to the imidazolidine ring (Figure 5). The imidazolidine ring is condensed with the tetrahydropyrazine ring in a manner that the pterin ring sits roughly parallel but not in direct contact to the dezaisoalloxazine ring. Notably, $F_{420}H_2$ binding does not cause any visible conformational changes at methenyl-H_4MPT^+ despite the multiple contacts of the substrates. The three-membered ring of $F_{420}H_2$ is present in a bent (butterfly) conformation with a bending angle of ca. 25° assessed on the basis of a pyrimidinedione ring not being planar. Moreover, the C5 atom of the pyridine ring is slightly flapped to the *si*-face (Figure 5) corroborating the assumption of F_{420} in the reduced state present. This conformation of $F_{420}H_2$ appears to be stabilized or more likely induced by structural constraints. The central pyridine ring is kept in its position outside the plane by Pro73 whose rigid hydrophobic ring is directed toward its *re*-face and acts as a backstop (Figure 4B). The shortest distance of ca. 3.3 Å was detected between the Pro73 Cγ atom and the C5a atom of the pyridine ring. The strictly conserved Pro73 sits at the tip of an unusual loop following β-strand 67:71. This β-strand forms together with β-strand 4:10, the switch point of the β-sheet which represents a functionally important place in all α/β proteins and was already predicted as the F_{420} binding site on the basis of the structure without substrates bound (*5*). The pyrimidinedione ring of F_{420} is rotated away from methenyl-H_4MPT^+, in particular to evade its C12a methyl group but also to avoid a collision with Met44 that sits at its *re*-face. Notably, the polar atoms O4 and N3 of the pyrimidinedione ring are hydrogen-bonded to Asn13 and Val42, which also interact with methenyl-H_4MPT^+ and thereby clamp the cofactors together (Figure 4B). The Asn13 carbonyl group approaches the C5 atom of F_{420} to 3.9 Å and contributes together with residues Pro73, Met124, and Leu125 and especially with the voluminous rings of the substrates themselves to the encapsulation of the hydride transfer reaction against the bulk solvent. The hydroxybenzyl wing of the deazaisoalloxazine ring is pivoted away from methenyl-H_4MPT^+ to evade a collision between a hydroxybenzyl carbon of $F_{420}H_2$ and a pyrimidinone oxygen of methenyl-H_4MPT^+. Moreover, Met124 pushes against the aromatic ring from the *si*-face, and Asp99 pointing to the *re*-face forms a hydrogen bond to the hydroxyl group of the hydroxybenzyl ring by its carboxylate group (Figure 4B). The latter interaction might also ensure specificity against FMN and FAD. The invariant Asp99 (in analogy to Asp122), in addition, plays an important role in connecting the domain linker, $F_{420}H_2$, and the loop following β-strand 67:71 and is thereby involved to provide proximity between Pro73 and $F_{420}H_2$.

Interestingly, the butterfly conformation of F_{420} is a general feature of all F_{420} molecules observed in the crystal structures. The observed binding angles are ca. 26° for F_{420}-dependent secondary alcohol dehydrogenase (*33*), 27° for methylene-H_4MPT reductase (*18*, *34*), 8° for F_{420}:$NADP^+$ oxidoreductase (*18*), and 25° for Mtd. In all F_{420}-dependent enzymes structurally studied the wings of F_{420} are turned away from the hydride donor/acceptor, thereby ensuring minimal repulsive orbital overlapping. How bending modifies the redox potential of F_{420} and whether this effect substantially influences catalysis are unknown.

Hydride Transfer Reaction. The hydride transfer reaction of Mtd occurs in a completely preformed crevice accurately shaped to harbor both methenyl/ylene-H_4MPT and $F_{420}H_2$ as described. Methenyl/ylene-H_4MPT is more deeply buried than $F_{420}H_2$ and is presumably embedded into the crevice at first. Afterward, $F_{420}H_2$ enters the crevice and is bound to a great extent by interactions to methenyl/ylene-H_4MPT (Figure 4A). Various cocrystallization experiments with substrates and products support this kind of substrate-induced substrate binding as $F_{420}H_2$ was never found in the electron density map upon structure determination when methenyl/ylene-H_4MPT was not also present. The binding scenario postulated was not expected as the binding sequence is reversed in methylene-H_4MPT reductase (*34*) which reversibly converts methylene- to methyl-H_4MPT via $F_{420}H_2$.

The methylene-H_4MPT and deazaisoalloxazine rings are oriented in the crevice such that the *re*-face of methylene-H_4MPT faces the *si*-face of $F_{420}H_2$, thus confirming the previously determined stereospecificity of the hydride transfer in solution (*35*) (Figure 1). Although the active site architecture only allows methenyl/ylene-H_4MPT and F_{420} binding in the found orientations and thereby explains the observed stereochemistry for Mtd in structural terms, the fundamental question why all F_{420}-dependent enzymes and all methylene-H_4MPT dehydrogenases exclusively exchange the *proS* and *proR* hydrogens, respectively (in contrast to FAD and NADP), remains unanswered. While no plausible hypothesis for explaining the *si*-face specificity of F_{420}-dependent enzymes exists, semiempirical quantum mechanical calculations on methenyl/ylene-H_4MPT resulted in a lower energy for *proR* hydrogen activation which might predetermine the *re*-face specificity (*8*).

The imidazolidine and pyridine rings of methenyl/ylene-H_4MPT and $F_{420}H_2$, respectively, are laterally shifted against each other in a manner that the hydride-transferring and a few neighboring atoms of the ring lie on top of each other (Figures 4 and 5). The angles between the planes of the catalytic rings are 165−170°, implying a van der Waals contact between many of their atoms. The shortest distance of ca. 2.7 Å is found between the hydride-transferring C14a and C5 atoms, suggesting a fairly accurate picture of the position and conformation of the substrates prior to the chemical event. This finding allows us a reliable modeling of the positions of the C14a and C5 hydrogen atoms largely determined by the coordinates of the ring structures (Figure 5). Accordingly, the modeled *proS* hydrogen at the C5 atom of $F_{420}H_2$ points toward the C14a atom, and the modeled *proR* hydrogen of the C14a atom of methylene-H_4MPT points toward $F_{420}H_2$. Their distance would be ca. 0.5 Å, which might be (partly) overcome by a tunneling process which was established for several hydride-transferring enzymes on the basis of quantum mechanical combined with molecular dynamics calculations (*36*, *37*). Notably, no amino acid residue appears to be directly involved in the hydride transfer process, but a few aforementioned residues are involved in shielding it from bulk solvent.

The major challenge for the polypeptide chain is to bind and adjust the bulky methenyl-H_4MPT^+ and $F_{420}H_2$ for an optimal hydride transfer, which is accomplished by a concerted action of many residues (Figure 4). This task is, however, not realized by the frequently observed substrate-induced (induced-fit) conformational change of the polypeptide chain. The action of Mtd rather provides a textbook example for a polypeptide-induced conformational change of the substrates. The amazingly fixed active site crevice is well suited to impose constraints on the

conformation of the relatively deformable multicyclic rings, which is essential to create a geometrically reasonable contact between the hydride-transferring atoms on one hand and to prevent collisions between the bulky rings on the other. The butterfly conformation of F_{420} and the extended conformation of both methenyl-H_4MPT^+ and methylene-H_4MPT are the visible outcomes of these constraints (Figure 3). For example, a kink between the pterin and the imidazolidine rings as found in solution (*8*) and in the formaldehyde activating enzymes (*30*) would (dependent on its direction) either cause a clash with F_{420} or separate the C5 atoms of F_{420} and C14a atoms of methylene-H_4MPT too far for a hydride exchange at biological rates. Besides the described rather indirect function, the polypeptide scaffold might, in addition, actively enhance catalytic efficiency by compressing the hydride-transferring atoms toward each other (Figure 4) and by modulating the imidazolidine conformation and the configuration of individual ring atoms as suggested for the N10 atom in methylene-H_4MPT of [Fe] hydrogenase (*38*). Unfortunately, the resolutions of the binary and ternary complexes are not sufficient to identify distances with high accuracy, tiny distortions of the rings, and the configuration of individual atoms involved in catalysis. Related stereoelectronic effects are described for other enzymes catalyzing a hydride transfer reaction between two bulky substrates as, for example, for glutathione reductase (*39*) and for F_{420}-NADPH oxidoreductase (*18*).

ACKNOWLEDGMENT

We thank Hartmut Michel for continuous support, Stefan Schiesser and Thomas Carell (Ludwig-Maximilian-Universität, München) for FO synthesis, and the staff of PXII at the Swiss-Light-Source in Villigen (Switzerland) for help during data collection.

REFERENCES

1. Thauer, R. K. (1998) Biochemistry of methanogenesis: a tribute to Marjory Stephenson. 1998 Marjory Stephenson Prize Lecture. *Microbiology 144* (Part 9), 2377–2406.
2. van Beelen, P., Stassen, A. P., Bosch, J. W., Vogels, G. D., Guijt, W., and Haasnoot, C. A. (1984) Elucidation of the structure of methanopterin, a coenzyme from *Methanobacterium thermoautotrophicum*, using two-dimensional nuclear-magnetic-resonance techniques. *Eur. J. Biochem. 138*, 563–571.
3. Escalante-Semerena, J. C., Rinehart, K. L.Jr., and Wolfe, R. S. (1984) Tetrahydromethanopterin, a carbon carrier in methanogenesis. *J. Biol. Chem. 259*, 9447–9455.
4. Hartzell, P. L., Zvilius, G., Escalante-Semerena, J. C., and Donnelly, M. I. (1985) Coenzyme F420 dependence of the methylenetetrahydromethanopterin dehydrogenase of *Methanobacterium thermoautotrophicum*. *Biochem. Biophys. Res. Commun. 133*, 884–890.
5. Hagemeier, C. H., Shima, S., Thauer, R. K., Bourenkov, G., Bartunik, H. D., and Ermler, U. (2003) Coenzyme F420-dependent methylenetetrahydromethanopterin dehydrogenase (Mtd) from *Methanopyrus kandleri*: a methanogenic enzyme with an unusual quarternary structure. *J. Mol. Biol. 332*, 1047–1057.
6. Shima, S., Pilak, O., Vogt, S., Schick, M., Stagni, M. S., Meyer-Klaucke, W., Warkentin, E., Thauer, R. K., and Ermler, U. (2008) The crystal structure of [Fe]-hydrogenase reveals the geometry of the active site. *Science 321*, 572–575.
7. Ermler, U., Hagemeier, C. H., Roth, A., Demmer, U., Grabarse, W., Warkentin, E., and Vorholt, J. A. (2002) Structure of methylenetetrahydromethanopterin dehydrogenase from *Methylobacterium extorquens* AM1. *Structure 10*, 1127–1137.
8. Bartoschek, S., Buurman, G., Thauer, R. K., Geierstanger, B. H., Weyrauch, J. P., Griesinger, C., Nilges, M., Hutter, M. C., and Helms, V. (2001) Re-face stereospecificity of methylenetetrahydromethan opterin and methylenetetrahydrofolate dehydrogenases is predetermined by intrinsic properties of the substrate. *ChemBioChem 2*, 530–541.
9. Allaire, M., Li, Y., MacKenzie, R. E., and Cygler, M. (1998) The 3-D structure of a folate-dependent dehydrogenase/cyclohydrolase bifunctional enzyme at 1.5 Å resolution. *Structure 6*, 173–182.
10. Maden, B. E. (2000) Tetrahydrofolate and tetrahydromethanopterin compared: functionally distinct carriers in C1 metabolism. *Biochem. J. 350* (Part 3), 609–629.
11. Kurr, M., Huber, R., Koenig, H., Jannasch, H. W., Fricke, H., Trineone, A., Kristjansson, J. K., and Stetter, K. O. (1991) *Methanopyrus kandleri*, gen. and sp. nov. represents a novel group of hyperthermophilic methanogens, growing at 110° C. *Arch. Microbiol. 156*, 239.
12. Klein, A. R., Koch, J., Stetter, K. O., and Thauer, R. K. (1993) Two N5,N10-methylenetetrahydromethanopterin dehydrogenases in the extreme thermophile *Methanopyrus kandleri*: characterization of the coenzyme F420-dependent enzyme. *Arch. Microbiol. 160*, 186–192.
13. Mukhopadhyay, B., and Daniels, L. (1989) Aerobic purification of N5,N10-methylenetetrahydromethanopterin dehydrogenase, separated from N5,N10-methylenetetrahydromethanopterin cyclohydrolase, from *Methanobacterium thermoautotrophicum* strain Marburg. *Can. J. Microbiol. 35*, 499–507.
14. Te Brommelstroet, B. W., Geerts, W. J., Keltjens, J. T., van der Drift, C., and Vogels, G. D. (1991) Purification and properties of 5,10-methylenetetrahydromethanopterin dehydrogenase and 5,10-methylenetetrahydromethanopterin reductase, two coenzyme F420-dependent enzymes, from *Methanosarcina barkeri*. *Biochim. Biophys. Acta 1079*, 293–302.
15. Klein, A. R., and Thauer, R. K. (1997) Overexpression of the coenzyme-F420-dependent N5,N10-methylenetetrahydromethanopterin dehydrogenase gene from the hyperthermophilic *Methanopyrus kandleri*. *Eur. J. Biochem. 245*, 386–391.
16. Karplus, P. A., and Schulz, G. E. (1989) Substrate binding and catalysis by glutathione reductase as derived from refined enzyme: substrate crystal structures at 2 Å resolution. *J. Mol. Biol. 210*, 163–180.
17. Pejchal, R., Sargeant, R., and Ludwig, M. L. (2005) Structures of NADH and CH_3-H_4folate complexes of *Escherichia coli* methylenetetrahydrofolate reductase reveal a spartan strategy for a ping-pong reaction. *Biochemistry 44*, 11447–11457.
18. Warkentin, E., Mamat, B., Sordel-Klippert, M., Wicke, M., Thauer, R. K., Iwata, M., Iwata, S., Ermler, U., and Shima, S. (2001) Structures of F420H2:$NADP^+$ oxidoreductase with and without its substrates bound. *EMBO J. 20*, 6561–6569.
19. Sawaya, M. R., and Kraut, J. (1997) Loop and subdomain movements in the mechanism of *Escherichia coli* dihydrofolate reductase: crystallographic evidence. *Biochemistry 36*, 586–603.
20. Hagemeier, C. H., Shima, S., Warkentin, E., Thauer, R. K., and Ermler, U. (2003) Coenzyme F420-dependent methylenetetrahydromethanopterin dehydrogenase from *Methanopyrus kandleri*: the selenomethionine-labelled and non-labelled enzyme crystallized in two different forms. *Acta Crystallogr., Sect. D: Biol. Crystallogr. 59*, 1653–1655.
21. Shima, S., and Thauer, R. K. (2001) Tetrahydromethanopterin-specific enzymes from *Methanopyrus kandleri*. *Methods Enzymol. 331*, 317–353.
22. Otwinowski, Z. M., W. (1997) Processing of X-ray diffraction data collected in oscillation mode. *Macromol. Crystallogr. 276*, 10.
23. Kabsch, W. (1993) Automatic processing of rotation diffraction data from crystals of initially unknown symmetry and cell constants. *J. Appl. Crystallogr. 26*, 795–800.
24. Navaza, J. (1994) AMORE: an automated package for molecular replacement. *Acta Crystallogr., Sect. A: Biol. Crystallogr. 50*, 7.
25. McCoy, A. J., Grosse-Kunstleve, R. W., Adams, P. D., Winn, M. D., Storoni, L. C., and Read, R. J. (2007) Phaser crystallographic software. *J. Appl. Crystallogr. 40*, 658–674.
26. Murshudov, G. N., Vagin, A. A., and Dodson, E. J. (1997) Refinement of macromolecular structures by the maximum-likelihood method. *Acta Crystallogr. D 53*, 240–255.
27. Emsley, P., and Cowtan, K. (2004) Coot: model-building tools for molecular graphics. *Acta Crystallogr., Sect. D: Biol. Crystallogr. 60*, 2126–2132.
28. Laskowski, R. A., Moss, D. S., and Thornton, J. M. (1993) Main-chain bond lengths and bond angles in protein structures. *J. Mol. Biol. 231*, 1049–1067.
29. Holm, L., and Sander, C. (1993) Protein structure comparison by alignment of distance matrices. *J. Mol. Biol. 233*, 123–138.
30. Acharya, P., Goenrich, M., Hagemeier, C. H., Demmer, U., Vorholt, J. A., Thauer, R. K., and Ermler, U. (2005) How an enzyme binds the C1 carrier tetrahydromethanopterin. Structure of the tetrahydromethanopterin-dependent formaldehyde-activating enzyme (Fae)

from *Methylobacterium extorquens* AM1. *J. Biol. Chem. 280*, 13712–13719.
31. Hyatt, D. C., Maley, F., and Montfort, W. R. (1997) Use of strain in a stereospecific catalytic mechanism: crystal structures of *Escherichia coli* thymidylate synthase bound to FdUMP and methylenetetrahydrofolate. *Biochemistry 36*, 4585–4594.
32. Trimmer, E. E., Ballou, D. P., Ludwig, M. L., and Matthews, R. G. (2001) Folate activation and catalysis in methylenetetrahydrofolate reductase from *Escherichia coli*: roles for aspartate 120 and glutamate 28. *Biochemistry 40*, 6216–6226.
33. Aufhammer, S. W., Warkentin, E., Berk, H., Shima, S., Thauer, R. K., and Ermler, U. (2004) Coenzyme binding in F420-dependent secondary alcohol dehydrogenase, a member of the bacterial luciferase family. *Structure 12*, 361–370.
34. Aufhammer, S. W., Warkentin, E., Ermler, U., Hagemeier, C. H., Thauer, R. K., and Shima, S. (2005) Crystal structure of methylenetetrahydromethanopterin reductase (Mer) in complex with coenzyme F420: architecture of the F420/FMN binding site of enzymes within the nonprolyl cis-peptide containing bacterial luciferase family. *Protein Sci. 14*, 1840–1849.
35. Klein, A. R., and Thauer, R. K. (1995) Re-face specificity at C14a of methylenetetrahydromethanopterin and Si-face specificity at C5 of coenzyme F420 for coenzyme F420-dependent methylenetetrahydromethanopterin dehydrogenase from methanogenic Archaea. *Eur. J. Biochem. 227*, 169–174.
36. Masgrau, L., Ranaghan, K. E., Scrutton, N. S., Mulholland, A. J., and Sutcliffe, M. J. (2007) Tunneling and classical paths for proton transfer in an enzyme reaction dominated by tunneling: oxidation of tryptamine by aromatic amine dehydrogenase. *J. Phys. Chem. B 111*, 3032–3047.
37. Nagel, Z. D., and Klinman, J. P. (2006) Tunneling and dynamics in enzymatic hydride transfer. *Chem. Rev. 106*, 3095–3118.
38. Bartoschek, S., Buurman, G., Geierstanger, B. H., Lapham, J., and Griesinger, C. (2003) Measurement and ab initio calculation of CSA/dipole-dipole cross-correlated relaxation provide insight into the mechanism of a H2-forming dehydrogenase. *J. Am. Chem. Soc. 125*, 13308–13309.
39. Berkholz, D. S., Faber, H. R., Savvides, S. N., and Karplus, P. A. (2008) Catalytic cycle of human glutathione reductase near 1 Å resolution. *J. Mol. Biol. 382*, 371–384.